RAA 2015 Vol. **15** No. **7**, 1027–1035 doi: 10.1088/1674–4527/15/7/010
http://www.raa-journal.org *http://www.iop.org/journals/raa*

Research in Astronomy and Astrophysics

Propagating disturbances along a coronal loop from simultaneous EUV imaging and spectroscopic observations

Ajanta Datta[1,3], S. Krishna Prasad[2] and Dipankar Banerjee[3]

[1] HKBK College of Engineering, Nagawara, Bangalore 560 045, India; *ajanta@iiap.res.in*
[2] Astrophysics Research Centre, School of Mathematics and Physics, Queen's University Belfast, Belfast BT7 1NN, UK
[3] Indian Institute of Astrophysics, Bangalore 560034, India

Received 2014 September 14; accepted 2014 November 26

Abstract Propagating disturbances (PDs) were studied along an active region loop using simultaneous imaging and spectroscopy. An image sequence recorded in the Fe IX/Fe X 171Å channel, from *TRACE* and spectral data in the Si XII 520.6 Å line obtained from CDS/*SOHO*, are analyzed. A space-time map constructed from the *TRACE* image sequence shows the presence of PDs close to the loop foot point propagating with an apparent speed of 39 km s^{-1}. The periodicity was found to be 5.4 min. The corresponding spectroscopic data from CDS, at a location away from the foot point, show oscillations in all three line parameters roughly at the same period. At locations farther from the foot point, the line width oscillation seems to disappear while the Doppler velocity oscillation becomes prominent. We attribute this to the signature of propagating slow waves that get affected by flows/other events close to the foot point. Spectral line profiles do not show much asymmetry, however, it is difficult to infer anything due to the broadened Gaussian shape of the CDS line profiles.

Key words: Sun: corona — oscillations — UV radiation — imaging spectroscopy

1 INTRODUCTION

Propagating Disturbances (PDs) are well observed phenomena along different coronal structures. The first observational report on PDs along coronal loops was by Berghmans & Clette (1999). Since then a number of authors have studied PDs in active region loops (e.g., see the review by de Moortel 2009; Krishna Prasad et al. 2012b; Su et al. 2013). Such studies have gained importance recently for their probable role in coronal heating (De Moortel 2008) and for their application as a diagnostic tool through coronal seismology (Uchida 1970; Roberts et al. 1984; De Moortel & Nakariakov 2012). PDs are also identified from the analysis of spectroscopic data (e.g., Banerjee et al. 2000, 2001, 2009; Wang et al. 2009b,a) through the detection of oscillations in intensity and Doppler velocity. They are mostly interpreted as propagating slow magneto-acoustic waves based on the observed properties.

Imaging and spectroscopic observations are unique in their own way, but a combined study gives a better understanding of the observed PDs. O'Shea et al. (2002) reported both upward and downward PDs in the upper corona from a combined analysis of data from *Transition Region and Coronal Explorer* (*TRACE*) and Coronal Diagnostic Spectrometer (CDS)/*Solar and Heliospheric*

Observatory (SOHO). Del Zanna (2003) has shown a clear relation between emissions in the corona, the transition region and the photosphere using observations from *TRACE* and CDS/*SOHO*. Marsh et al. (2003, 2004) detected slow magneto-acoustic waves with a periodicity of 5 min along coronal loops using the same set of instruments. Recently, De Pontieu & McIntosh (2010) studied PDs using data from *TRACE* and *Hinode*/EIS and suggested that the interpretation of PDs as waves is not unique. They further indicate that a quasiperiodic upflow can give similar observational evidence in intensity and can be misinterpreted when studied from the imaging data alone. These authors also found that the usual intensity and velocity oscillations expected for the slow waves are in fact accompanied by in-phase oscillations in line width and the spectral line profiles periodically show a significant blue-shifted component, a signature of quasiperiodic upflow. Tian et al. (2011) have also observed these in-phase oscillations in spectral line intensity, Doppler velocity, and line width suggesting that the observed oscillatory behavior is due to quasiperiodic upflows. However, the flow interpretation is not supported by all. Verwichte et al. (2010) have demonstrated that slow waves can cause line asymmetries when averaged over a time period. Wang et al. (2012) observed blue-wing asymmetry in hot coronal lines and suggested that the propagating intensity and Doppler velocity oscillations are due to variations of the core component, not due to the high velocity minor component. This argument supports the slow wave interpretation. Krishna Prasad et al. (2012a) have studied PDs using combined observations from *Hinode*/EIS and AIA/SDO. They have observed oscillations in spectral line intensity and Doppler velocity but not in line width. They also did not find any visible asymmetry in the line profile.

Nishizuka & Hara (2011) have reported, using data from *Hinode*/EIS, both continuous outflows and waves by analyzing the line profiles at the base and higher locations of the outflow. Ofman et al. (2012) and Wang et al. (2013) have done three dimensional modeling of a bipolar Active Region (AR) and observed that excitation of damped slow magneto-acoustic waves that propagate along the loops is possibly due to the onset of flows with subsonic speeds. In the present scenario of several views of PDs, combined analyses have become more relevant. Different modes of observations highlight different aspects that can lead to a better understanding of the nature of the PDs.

In this paper we have studied the nature of PDs along an AR coronal loop when it was at a position off the limb, by combining EUV images from *TRACE* and spectroscopic data from CDS. PDs have been detected near the foot point of the loop from the *TRACE* image. The spectral parameters, peak intensity, Doppler velocity, and line width, at another position along the loop, have been analyzed to draw further conclusions about their nature.

In Section 2 we have described the details of the data and the processing methods used in this study. In Section 3 we have presented the analysis techniques and the results obtained. We have provided a detailed discussion of the results and the conclusions in Section 4.

2 DATA

The data used in this analysis are part of a Joint Observational Programme (JOP 165). In this campaign an AR (AR 10457) was followed over a period of 12 days (2003 September 5 to 2003 September 17) during its journey from one limb to the other and involves observations from *TRACE*, CDS and the *Michelson Doppler Imager* (MDI) on board *SOHO*. *TRACE* collects images of solar plasma at different temperatures ranging from 10^4 to 10^7 K, using several UV/EUV/visible channels. The CDS performs EUV spectroscopy for plasma temperatures ranging from 2×10^4 to 3×10^6 K. The data obtained on 2003 September 5, when the AR was at a position off the limb, are used in the current work. The *TRACE* data consist of an image sequence composed of 28 frames taken with 512 pixels arranged in a square array, recorded in the Fe IX/Fe X 171Å channel, during 17:02 UT to 17:32 UT. The field of view is centered at (–980″, –132″). These data have been reduced using the routine *trace_prep.pro* of **sswidl** following the standard procedure. The final pixel size and cadence of the data are 1.0″and 60 s respectively. The CDS data consist of a raster scan and five sit and stare

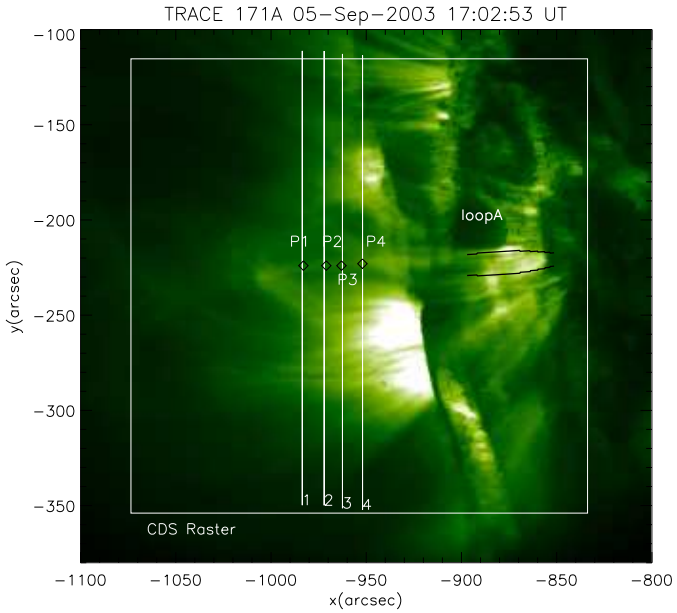

Fig. 1 *TRACE* image showing AR 10457 at a position off the limb on 2003 September 5. A section of the loop under investigation is marked as Loop A with black lines. The white box indicates the field of view of the CDS raster scan and the vertical lines mark the sit and stare slit positions. Black diamonds indicate the pixel positions on different slits where Loop A intersects.

observations. The raster scan was taken from 15:10 UT to 15:32 UT using the Mg IX (368.07 Å) line. This 60×72 pixel scan has its lower left corner at (–1081″, –363″). The sit and stare observations were taken between 16:02 UT and 18:02 UT, with half an hour of observing time at each of the slit positions. All the slit positions are separated by $10''$ with the one closest to the limb being located at solar-X $\approx -949''$. Four out of the five sit and stare observations taken in the coronal Si XII 520.6 Å ($\log\ T_e = 6.3$) line are used in this analysis. The observations were made in five other lines which were not useful either because they were transition region lines with a poor signal-to-noise that were taken off the limb or because the oscillations in those lines were inconsistent. Standard CDS software was used for the initial preparation of the data. Since the data were observed in the post recovery phase of *SOHO*, the spectral profiles were fitted with a broadened Gaussian[1]. The final pixel resolution and the cadence of the data are $4.0'' \times 3.3''$and 21 s, respectively. Proper alignments between different data sets play a major role when observations from multiple instruments are used in the analysis. The CDS raster in the Mg IX line and the corresponding subfield from the *TRACE* image are co-aligned using intensity cross correlation and the slit positions are corrected by the appropriate offset. The final CDS slit positions and the field of view of the raster scan are shown on a subfield of the *TRACE* image in Figure 1.

3 ANALYSIS AND RESULTS

In this section we discuss the techniques used to detect the PD, and to determine the periodicities of oscillations and other properties, from both *TRACE* and CDS/*SOHO* data.

[1] After the recovery of *SOHO*, the line profiles of CDS were found to have acquired substantial wings. A function was then developed to accommodate these enhanced wings over a Gaussian and named broadened Gaussian. Refer to CDS Software Note No. 53 (*http://solar.bnsc.rl.ac.uk/swnotes/cds_swnote_53.pdf*) for more information.

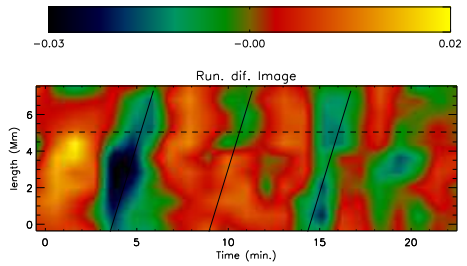

Fig. 2 Enhanced space-time map created from the section of Loop A marked by black lines in Figure 1. The scale of the color bar indicates the percentage of oscillation. The dashed line marks the location where wavelet analysis is done to determine the periodicity. The slope of the slanted solid lines drawn along the dark ridges gives an estimate for the propagation speed.

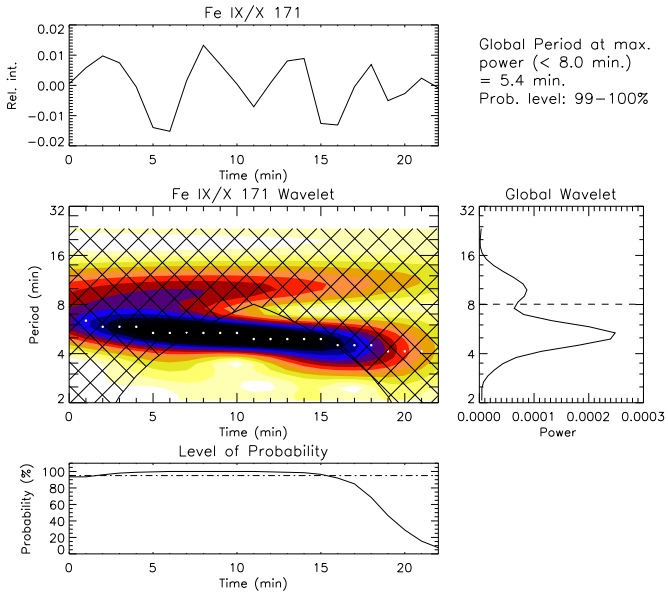

Fig. 3 Wavelet plot for intensity variations observed from *TRACE* at an arbitrarily chosen pixel location along Loop A (Fig. 1). Each panel consists of the detrended light curve (*top left*), wavelet spectrum (*middle left*), level of probability (*lower left*) and power spectrum (*right*).

We have chosen an AR loop, marked as Loop A in Figure 1, for this study. The loop foot point is located at solar-X $\approx -860''$. A section of the loop close to its foot point is analyzed to find PDs from the *TRACE* data. A space-time map is created following a method similar to that explained in Krishna Prasad et al. (2012a) and De Moortel et al. (2000). From each time frame, we create a 1-d array of intensity along the loop, by averaging and normalizing over pixels along the cross section of the loop which are then stacked together to generate the desired map. This map was then processed by detrending and normalizing, to enhance the visibility of the bands. An eight point running average has been used for detrending, which should filter out oscillations with periodicities longer than 8 min. The final processed space-time map is shown in Figure 2. Alternate bright and dark fringes visible in this map with a positive slope indicate the presence of PDs propagating outward. To determine the periodicity, we have done wavelet analysis (Torrence & Compo 1998) at an arbitrarily chosen pixel

(shown by the dotted line on this map) approximately at a distance of 5 Mm from the loop foot point. The results of this analysis are shown in Figure 3. A running average of 15 points (≈ 15 min) has been subtracted from the original *TRACE* light curve to eliminate the background trend. This detrended light curve is then subjected to the wavelet analysis which is shown in the upper panel of the wavelet plot. The Morlet wavelet function, a complex sine wave modulated by a Gaussian, is chosen as the Mother wavelet function. The middle left panel shows the actual wavelet plot which displays the presence of oscillations at different periodicities and their evolution with time. The cone of influence (Torrence & Compo 1998) is marked by the cross hatched region. The periodicities, obtained in this region, are not reliable due to edge effects. The power at different periods averaged over time is shown in the global wavelet plot, in the right panel. A probability estimate was calculated using the randomization method with 200 permutations as outlined in detail by Banerjee et al. (2001). The variation of the probability estimate associated with the maximum power at each time in the wavelet-power spectrum is shown in the lower left plot. The dash-dotted line in this plot marks the 95% probability level. The periodicity of the PD is found to be 5.4 min. To calculate the propagation speed, a straight line is drawn parallel to the ridges and its slope is estimated. Three parallel slanted lines are drawn on the space-time map in Figure 2, to indicate this. The positioning of these lines along the adjacent dark bands confirms the periodicity, which is obtained from wavelet analysis. The estimated propagation speed is about 39 km s^{-1}.

Spectral data from the CDS sit and stare observations are also analyzed to understand the nature of the detected PDs along Loop A. The sit and stare slits of CDS are crossing Loop A perpendicularly. The pixel locations of the crossing points of the loop and CDS slits are identified and marked as P4 (on Slit 4, Solar-X$= -949''$), P3 (on Slit 3, Solar-X$= -959''$), P2 (on Slit 2, Solar-X$= -969''$) and P1 (on Slit 1, Solar-X$= -980''$) in Figure 1. Wavelet analysis is done at these locations to detect oscillatory behavior in spectral line intensity, Doppler velocity and line width. The analysis procedure followed is similar to the one described above. CDS time series are smoothed over two temporal points (which removes variation less than 42 s) and a running average of 25 points ($\approx$9 min) has been subtracted to eliminate the background trend before applying the wavelet technique. The results corresponding to the intensity, Doppler velocity and line width, at location P4, are shown in Figure 4. The primary periods of oscillation were found to be 4.1 min and 3.5 min for intensity and Doppler velocity, respectively. The wavelet plots show the presence of a few other periodicities in both the cases. The line width at this location displays a strong oscillation of 5.3 min. Location P3 demands special attention as the observation time (17:02 UT to 17:32 UT) matches that of the image sequence taken by *TRACE*. Here, we found oscillations with a period of 5.8 min for both line intensity and Doppler velocity. The line width variation also shows a periodicity of 5.3 min, close to this value. Corresponding wavelet plots are shown in Figure 5. These values are also close to what is found from the *TRACE* image analysis. By combining *TRACE* and CDS in our study, we are able to determine the periodicities of PDs simultaneously at the foot point and at a distance of approximately 71 Mm away from the foot point. At location P2 (≈ 78 Mm away from the loop foot point),

Table 1 Periodicities and amplitudes of oscillations along Loop A as obtained from wavelet analysis. Results are listed from *TRACE* 171 images and from four CDS sit and stare observations.

Emission line/ Channel	Approximate distance from the foot point (Mm)	Intensity amplitude (%)	Intensity period (min)	Velocity amplitude (km s^{-1})	Velocity period (min)	Line width amplitude (%)	Line width period (min)
Fe IX/Fe X 171Å	5	0.5	5.4	–	–	–	–
Si XII 520.6 Å	64	1.4	4.1	1.5	3.5	0.5	5.3
Si XII 520.6 Å	71	1.6	5.8	1.6	5.8	0.5	5.3
Si XII 520.6 Å	78	2.4	4.9	1.6	9.0/4.1	0.8	7.5/3.5
Si XII 520.6 Å	86	–	–	1.5	6.3	–	–

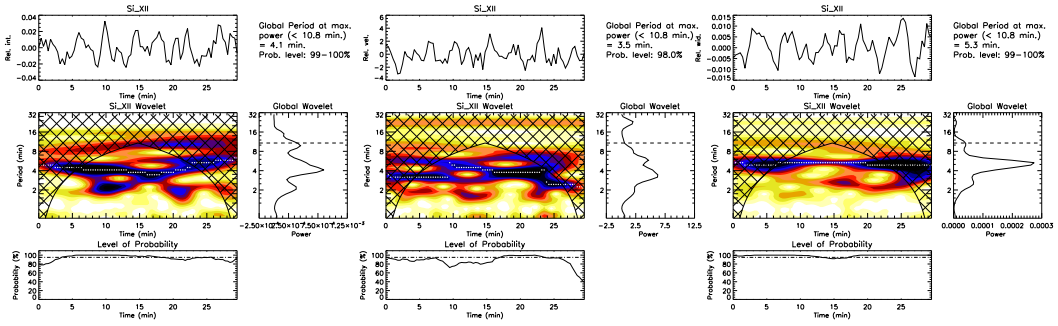

Fig. 4 Wavelet analysis of variations in intensity (*left panel*), Doppler velocity (*middle panel*) and line width (*right panel*) from CDS Slit 4. Panel descriptions are the same as those explained in Fig. 3.

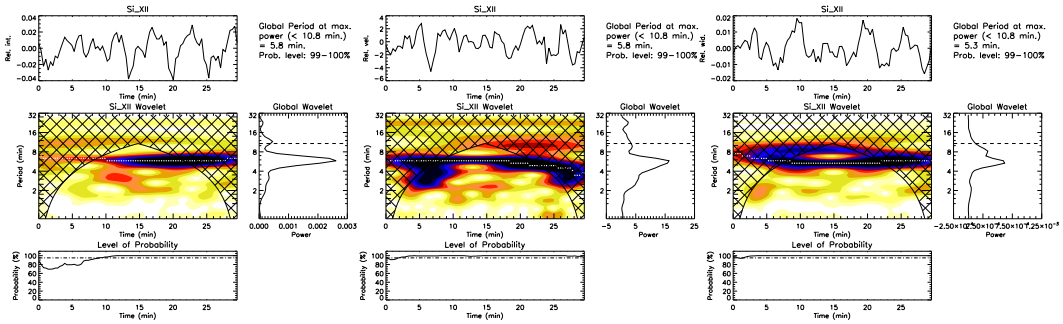

Fig. 5 Wavelet analysis of variations in intensity (*left panel*), Doppler velocity (*middle panel*) and line width (*right panel*) from CDS Slit 3. Panel descriptions are the same as those explained in Fig. 3.

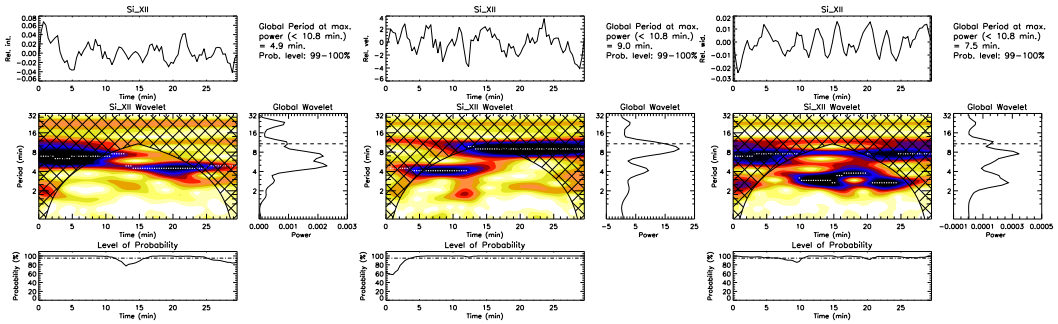

Fig. 6 Wavelet analysis of variations in intensity (*left panel*), Doppler velocity (*middle panel*) and line width (*right panel*) from CDS Slit 2. Panel descriptions are the same as those explained in Fig. 3.

the intensity and Doppler velocity variations show periodicities of 4.9 min and 9.0 min respectively, as shown in Figure 6.

The Doppler velocity oscillation also shows a second peak at 4.1 min. The oscillations in line width show the presence of two periods, 7.5 min and 3.5 min, with a broadened peak at the latter period. The broadened peak indicates the distribution of power over a range of periodicities, but the sharp peak in the global wavelet plot at P4 supports the presence of a dominant period in the

line width oscillation. As we move towards the loop apex, at location P1, a 6.3 min oscillation is observed in Doppler velocity while line intensity and line width do not show any clear sign of oscillation. The periodicities and amplitudes of the oscillations found at these locations along the loop are summarized in Table 1 for all the line parameters.

4 DISCUSSION

We studied the properties of PDs along an AR loop using data obtained through simultaneous imaging and spectroscopy. The periodicity and propagation speed of the PDs, as obtained from the imaging data, were found to be 5.4 min and 39 km s^{-1}, respectively. Although the imaging data do not show the PDs extending far along the loop, the spectroscopic data at four different locations away from the foot point show oscillations in all the three line parameters with a roughly similar period. It is possible that the broadband filters and the different sensitivity of the imaging instrument (*TRACE*) might have led to the non-detection of these low-amplitude oscillations at such distances (Krishna Prasad et al. 2012a). For instance, Wang et al. (2009a) observed PDs in the spectroscopic data obtained from *Hinode*/EIS but could not find them in the corresponding *TRACE* data, which they attributed to the lower sensitivity of the instrument. So, we believe the oscillations observed in the spectroscopic data (away from the foot point) and the PDs found from the imaging data (close to the foot point) are related, particularly since the periodicities are similar. The ≈5 min periodicity and the subsonic propagation speeds might suggest the PDs are due to propagating slow magneto-

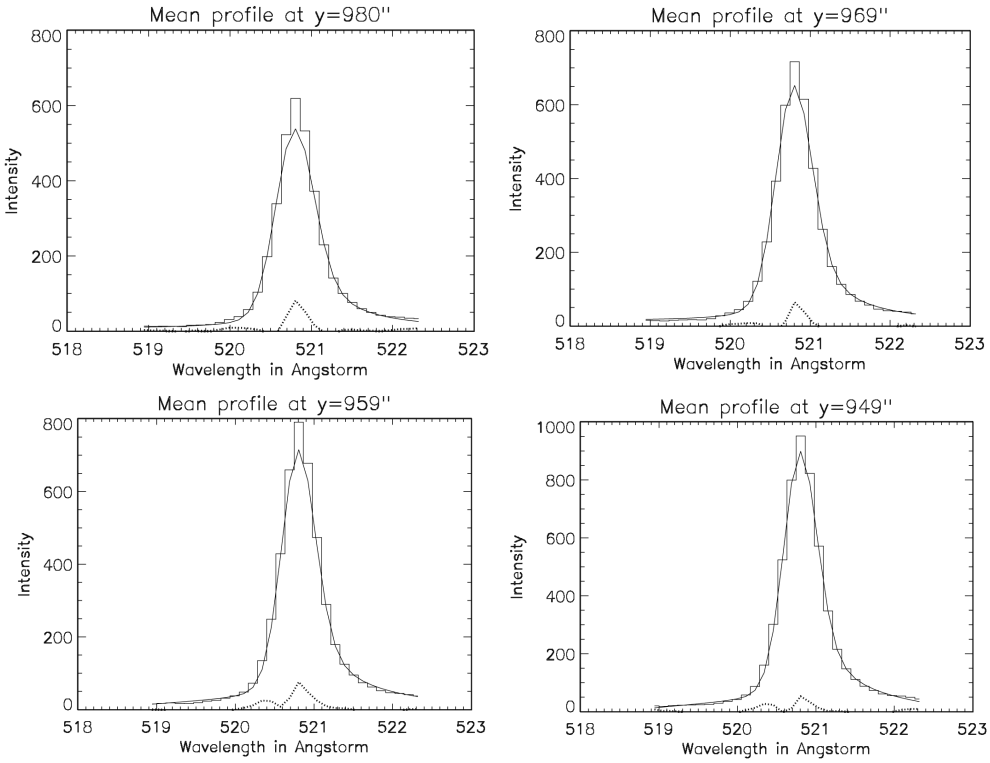

Fig. 7 Time averaged spectral profiles of the Si XII 520.6 Å line at the four analysis locations: P1 (*upper left*), P2 (*upper right*), P3 (*lower left*) and P4 (*lower right*). The solid line displays the best fit to the data using a broadened Gaussian function. The dotted line indicates the residual.

acoustic waves but the spectroscopic data show clear oscillations in line width as well. However, the oscillations in line width were prominent at location P4 which is relatively closer to the foot point and tend to show other periods as we move to P2 and no significant oscillation was detected at location P1. The Doppler velocity oscillations, on the other hand, show clearer peaks as we move towards P1. This might imply that wave-like behavior is more evident away from the foot point while the locations close to the foot point are affected by flows or some similar events. A cross-correlation analysis between intensity and Doppler velocity at these locations shows no clear correlation except at P3 where a phase lag of $\approx 84^\circ$ was found. The lack of clear correlation (which is expected) might be due to the presence of multiple periods but the phase lag found at P3 is difficult to interpret. The time averaged spectral line profiles at locations P1 to P4 are shown in Figure 7.

The data are fitted with a broadened Gaussian function along with a polynomial background. The overplotted solid lines in the figure represent the best fits to the data and the dotted line represents the residuals. These profiles do not show much asymmetry apart from the inherent red asymmetry expected for the post recovery NIS-2[2] spectra. It may be noted that averaging over time reduces the asymmetry caused by periodic upflows unlike the case of strong persistent upflows. So, we inspected a few individual profiles and they seem to show similar behavior. However, a clean spectral profile (with no blends or inherent asymmetries) with very good signal-to-noise is required to identify the low-amplitude blue wing enhancements due to quasiperiodic upflows. Simultaneous imaging and spectroscopic observations with better signal-to-noise are therefore crucial to improve our understanding of these PDs. The origin and damping of these disturbances are another important aspect that might require simultaneous observations in different layers from the photosphere to corona. The recent launch of IRIS (De Pontieu et al. 2014) can complete the currently available instruments that provide such coverage.

Acknowledgements The *Transition Region and Coronal Explorer*, *TRACE*, is a mission of the Stanford-Lockheed Institute for Space Research, and part of the NASA Small Explorer program. CDS is a part of *SOHO*, the *Solar and Heliospheric Observatory*, a project of international cooperation between ESA and NASA. The authors thank Subhankar Ray for useful conversations.

References

Banerjee, D., O'Shea, E., & Doyle, J. G. 2000, A&A, 355, 1152
Banerjee, D., O'Shea, E., Doyle, J. G., & Goossens, M. 2001, A&A, 371, 1137
Banerjee, D., Teriaca, L., Gupta, G. R., et al. 2009, A&A, 499, L29
Berghmans, D., & Clette, F. 1999, Sol. Phys., 186, 207
De Moortel, I. 2008, in European Solar Physics Meeting, 12, European Solar Physics Meeting, ed. H. Peter, 3
de Moortel, I. 2009, Space Sci. Rev., 149, 65
De Moortel, I., Ireland, J., & Walsh, R. W. 2000, A&A, 355, L23
De Moortel, I., & Nakariakov, V. M. 2012, Royal Society of London Philosophical Transactions Series A, 370, 3193
De Pontieu, B., & McIntosh, S. W. 2010, ApJ, 722, 1013
De Pontieu, B., Title, A. M., Lemen, J. R., et al. 2014, Sol. Phys., 289, 2733
Del Zanna, G. 2003, A&A, 406, L5
Krishna Prasad, S., Banerjee, D., & Singh, J. 2012a, Sol. Phys., 281, 67
Krishna Prasad, S., Banerjee, D., Van Doorsselaere, T., & Singh, J. 2012b, A&A, 546, A50
Marsh, M. S., Walsh, R. W., De Moortel, I., & Ireland, J. 2003, A&A, 404, L37

[2] NIS stands for the Normal Incidence Spectrometer that is part of CDS. NIS-2 refers to the second detector that records in the wavelength range 513–613 Å.

Marsh, M. S., Walsh, R. W., De Moortel, I., & Ireland, J. 2004, in ESA Special Publication, 547, SOHO 13 Waves, Oscillations and Small-Scale Transients Events in the Solar Atmosphere: Joint View from SOHO and TRACE, ed. H. Lacoste, 519
Nishizuka, N., & Hara, H. 2011, ApJ, 737, L43
Ofman, L., Wang, T. J., & Davila, J. M. 2012, ApJ, 754, 111
O'Shea, E., Muglach, K., & Fleck, B. 2002, A&A, 387, 642
Roberts, B., Edwin, P. M., & Benz, A. O. 1984, ApJ, 279, 857
Su, J. T., Liu, Y., Liu, S., et al. 2013, ApJ, 762, 42
Tian, H., McIntosh, S. W., & De Pontieu, B. 2011, ApJ, 727, L37
Torrence, C., & Compo, G. P. 1998, Bulletin of the American Meteorological Society, 79, 61
Uchida, Y. 1970, PASJ, 22, 341
Verwichte, E., Marsh, M., Foullon, C., et al. 2010, ApJ, 724, L194
Wang, T. J., Ofman, L., & Davila, J. M. 2009b, ApJ, 696, 1448
Wang, T. J., Ofman, L., Davila, J. M., & Mariska, J. T. 2009a, A&A, 503, L25
Wang, T., Ofman, L., & Davila, J. M. 2012, in Astronomical Society of the Pacific Conference Series, 455, 4th Hinode Science Meeting: Unsolved Problems and Recent Insights, eds. L. Bellot Rubio, F. Reale, & M. Carlsson, 227
Wang, T., Ofman, L., & Davila, J. M. 2013, ApJ, 775, L23